

## Analysis of the North Atlantic offshore energy flux from different reanalysis and hindcasts

Alday G., Matias; Raghavan, Vaibhav; Lavidas, George

**DOI**

[10.36688/ewtec-2023-140](https://doi.org/10.36688/ewtec-2023-140)

**Publication date**

2023

**Document Version**

Final published version

**Published in**

Vol. 15 (2023): Proceedings of the European Wave and Tidal Energy Conference

**Citation (APA)**

Alday G., M., Raghavan, V., & Lavidas, G. (2023). Analysis of the North Atlantic offshore energy flux from different reanalysis and hindcasts. In *Vol. 15 (2023): Proceedings of the European Wave and Tidal Energy Conference* (Vol. 15). Article 140 (Proceedings of the European Wave and Tidal Energy Conference). EWTEC. <https://doi.org/10.36688/ewtec-2023-140>

**Important note**

To cite this publication, please use the final published version (if applicable).  
Please check the document version above.

**Copyright**

Other than for strictly personal use, it is not permitted to download, forward or distribute the text or part of it, without the consent of the author(s) and/or copyright holder(s), unless the work is under an open content license such as Creative Commons.

**Takedown policy**

Please contact us and provide details if you believe this document breaches copyrights.  
We will remove access to the work immediately and investigate your claim.

***Green Open Access added to TU Delft Institutional Repository***

***'You share, we take care!' - Taverne project***

**<https://www.openaccess.nl/en/you-share-we-take-care>**

Otherwise as indicated in the copyright section: the publisher is the copyright holder of this work and the author uses the Dutch legislation to make this work public.

# Analysis of the North Atlantic offshore energy flux from different reanalysis and hindcasts

Matías Alday G., Vaibhav Raghavan and George Lavidas

**Abstract**—To date there is a wide range of wave reanalysis and hindcasts available to the scientific and engineering community which are commonly used for different applications, including downscaling or the estimation of the wave energy resource. These long datasets have been created using different combinations of forcing fields, physical parameterizations, and numerical choices (like spatial and spectral resolution). All these elements have a direct effect on the accuracy of the wave models' output and thus, they are one of the main reasons for the differences between these products. In the present study we analyze the significant wave heights and peak periods characteristics from a selection of global datasets. We additionally include results from a hindcast created using the WAVEWATCH III model, with adjustments specially aimed to reduce uncertainties of the wave energy resource along the Atlantic coasts of Europe. Models' output is compared with buoys and altimeter data from the latest ESA (European Space Agency) CCI Sea State V3 product. Preliminary validation of the hindcast we have generated for the North Atlantic already show an important bias reduction for wave heights in the 2.5 to 11.5 range compared to ERA5 wave product. Using the relevant wave parameters, we estimate the power density and quantify the differences between databases. Then, based on scatter diagrams obtained from the joint distributions of significant wave height and peak period, the differences in the power captured by a point absorber wave energy converter (WEC) related to different wave data sources will be quantified.

**Index Terms**—Wave energy flux, Hindcast, WAVEWATCH III, HAMS

## I. INTRODUCTION

**I**N recent years, there has been a substantial increase of studies and projects aimed to estimate the wave resource availability in different parts of the world using a variety of models and approaches ([1]–[5]). Typically, a resource assessment starts with an overview of the offshore wave climate using available hindcasts or reanalysis products. Based on these results, one may decide to downscale and develop a regional or coastal model to better represent wave conditions locally [6]. But these available datasets might largely differ from each other. Most likely, they have been created with different objectives in mind, and most important, using different combinations of forcing fields, physical

parameterizations, and numerical choices (like spatial and spectral resolution). In fact these are the most important factors affecting the accuracy of wave models' results (e.g.; [7]–[10]). It is thus of interest to verify how significant these differences are in the context of a wave resource assessment.

The main objective of this paper is to quantify the changes in the estimation of the offshore wave energy flux, in the North-East Atlantic, when different wave databases are employed. To that effect, we have selected 2 databases, the ERA5 reanalysis wave product [11], and the CFSR (Phase 2) hindcast [12], [13]. Additionally, using WAVEWATCH III<sup>®</sup> (WW3) [14], we have created a wave hindcast (from hereon MREL hindcast) to compare with the selected products. The MREL hindcast was developed with adjustments specially aimed to improve the model performance in European (Atlantic) waters, following the method proposed in [15]. At "basin" scale, the assessment of the different wave databases is done by comparing the simulated significant wave heights ( $H_s$ ) with altimeter data. For this, the ESA (European Space Agency) CCI Sea State V3 product is utilized [16].

Additionally, to verify how changes in the offshore energy flux might affect in intermediate to shallow waters, the differences in power captured by a C4 point absorber wave energy converter (PA-WEC) is considered. This estimation is done based on 1-year simulations from the MREL hindcast compared to the ERA5 wave product.

In this paper, we describe the databases used and general methods in section II. Then, in section III a brief description of the modelling approach used to obtain the power matrix from a PA-WEC is presented. Finally, we present the study's results in section IV followed by a brief discussion and conclusions in section V.

## II. MATERIALS AND METHOD

In the following sections, we provide a summarized description of the MREL hindcast developed for the North Atlantic, the wave reanalyses and altimeter data employed. Then, we specify the expressions used to compare the wave energy flux estimated with our simulations and the wave datasets selected.

### A. The MREL wave hindcast

The dataset was generated using WW3 implemented with a multi-grid 2-way nesting system ([17], [18]) that covers the North Atlantic from latitudes 0.25° to 80° North. The nesting setup consists of a base grid with a spacial resolution of 0.25° (N\_ATL-15M), a

© 2023 European Wave and Tidal Energy Conference. This paper has been subjected to single-blind peer review.

The work has been a part of the EU-SCORES project that has received funding from the European Union's Horizon 2020 research and innovation programme under grant agreement No 101036457.

M. Alday G. (e-mail: M.F.AldayGonzalez@tudelft.nl), V. Raghavan (e-mail: v.raghavan@tudelft.nl) and G. Lavidas (e-mail: g.lavidas@tudelft.nl) are with the Marine Renewable Energies Lab (MREL) from the Offshore Engineering Group in the Delft University of Technology, Stevinweg 1 2628 CN, Delft, The Netherlands.

Digital Object Identifier:  
<https://doi.org/10.36688/ewtec-2023-140>

regional grid that covers European waters with  $0.125^\circ$  (N\_ATL-8M), and a coastal high spatial resolution grid at  $0.03^\circ$  ( $\sim 2.3$  km; EU-3M, see Fig. 1). In terms of spectral resolution, 36 exponentially spaced frequencies are considered, from 0.034 to 0.95 Hz, with a 1.1 increment factor from one frequency to the next for all grids. In the directional space, 24 discrete directions are considered for the North Atlantic grid N\_ATL-15M (resolution of  $15^\circ$ ), and 36 directions for N\_ATL-8M and EU-2M (resolution of  $10^\circ$ ).

The forcing fields included in the model setup are:

- ERA5 winds [11] for wave generation.
- COPERNICUS-GLOBCURRENT surface global currents (product MULTI-OBS\_GLO\_PHY\_REP\_015\_004) applied only in N\_ATL-15M.
- The ice concentration from Ifremer SSMI-derived product [19] considering a 1 m constant thickness.
- And tidal levels and currents from the Atlantic-European North West Shelf-Ocean Physics Reanalysis (CMEMS product NWSHELF\_MULTIYEAR\_PHY\_004\_009). These ones used only in N\_ATL-8M and EU-2M.

The parameterizations for wind input and wave dissipation are taken from WW3's ST4 source terms package, described in [8]. Following the methodology proposed in [15], special adjustments were applied to the swell dissipation part of the ocean-atmosphere interactions parameterization from [8]. Additionally, wind corrections applied for wind speeds  $> 20.5$  m/s were introduced to partially correct the underestimation of high winds in products from the ECMWF IFS model [20] (see equation 6 in [15]). In this case, these adjustments were done to specifically improve the accuracy of the model results in the North-East Atlantic. To reduce computational cost, the Discrete Interaction Approximation (DIA) [21] was used to represent the 4-wave nonlinear interactions.

### B. Wave database

Two well known wave datasets are used to verify changes of the energy flux in deep waters. The ERA5 wave product and the CFSR hindcast (Phase 2).

The ERA5 global reanalysis was developed using 4D-Var data assimilation from the Integrated Forecast System (IFS) model cycle 41r2. The assimilation is applied in the atmospheric model (winds) and in the wave model WAM [22], which is coupled with the atmospheric one. The spectral discretization in the implemented version of WAM, considers 24 directions ( $15^\circ$  resolution) and 30 frequencies (0.03453 to 0.5478 Hz). The ERA5 wave product presents hourly data with a spatial resolution of  $0.5^\circ$ .

The CFSR hindcast was developed at NCEP (National Centers for Environmental Prediction) using WW3. The model is forced with CFSRR winds [23] and daily ice concentrations from the SMMR and SSMI. There is no wave data assimilation in the generation of this product (only in the forcing fields). Spectral discretization considers 50 frequencies (from 0.035 to 0.963 Hz) and 36 directional bins ( $10^\circ$  resolution). This

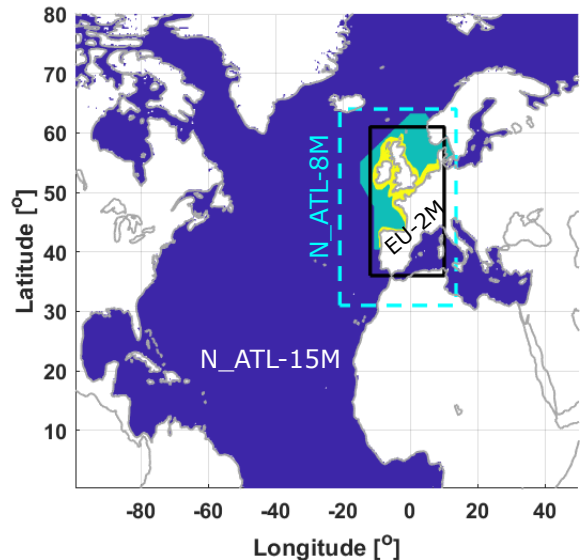


Fig. 1. Multi-grid 2-way nesting setup used in the generation of the MREL hindcast. Active N\_ATL-15M grid nodes in dark blue, in green active nodes from N\_ATL-8M grid, in yellow active nodes from the high resolution EU-2M grid.

product has 3-hourly data with a spatial resolution of  $0.5^\circ$ .

### C. Altimeter database

As mentioned in section I, the ESA CCI V3 altimeter L2P product [16] was selected to compare with  $H_s$  fields from the different wave datasets (including the MREL hindcast). The CCI V3 dataset provides 1 Hz averaged measurements of altimeter derived significant wave heights (SWH), which is equivalent to  $\sim 6$  km along-track resolution. The “denoised” SWH variable is used, which is obtained using the WHALES partial waveform retracking algorithm [24]. One interesting advantage of using the WHALES retracker, is its suitability for coastal applications (e.g.; [25], [26]).

It is important to mention that when comparing with altimeter derived wave heights, attention is paid to  $SWH \geq 1$  m. For  $H_s < 0.75$  m, altimeter measurements are not very accurate due to limited sampling of the signal associated with the radar bandwidth ([27], [28]).

### D. Statistical parameters

To assess the accuracy of the analyzed databases compared to altimeter data or buoy data, or between models, we use the following expressions: The Scatter Index (SI), and the Normalized Mean Bias (NMB).

$$SI(X) = \sqrt{\frac{\sum [(X_{\text{mod}} - \overline{X_{\text{mod}}}) - (X_{\text{obs}} - \overline{X_{\text{obs}}})]^2}{\sum X_{\text{obs}}^2}} \quad (1)$$

$$NMB(X) = \frac{\sum (X_{\text{mod}} - X_{\text{obs}})}{\sum X_{\text{obs}}} \quad (2)$$

In the expressions above, (1) and (2),  $X_{\text{obs}}$  and  $X_{\text{mod}}$  correspond to wave parameters obtained from measurements (altimeter in this case) and wave models

respectively (e.g;  $H_s$ , and the peak period  $T_p$ ). When (2) is use to compare 2 different databases we use the term Normalized Mean Differences (NMD).

When using altimeter data to compare with the modelled  $H_s$ , an along-track type analysis is employed. This implies the interpolation, in time and space, of the 4 closest points from the simulated  $H_s$  fields to collocate model data on the altimeter track. All comparisons with altimeter derived wave heights are done over a domain in the North-East Atlantic covering from longitude  $-40^\circ$  to  $37.5^\circ$ , and latitudes from  $15^\circ$  to  $80^\circ$ . The Mediterranean and Baltic Sea are excluded from the analysis.

### III. HYDRODYNAMIC MODEL OF THE WAVE ENERGY CONVERTER CORPOWER C4

This section briefly discusses the modelling of the wave energy converter Corpower C4 including its power matrix. A linearized sub-optimal power matrix considering viscous losses is derived here, which is then used to compare the power estimation from the considered databases.

#### A. Device Description

The Corpower C4 device (shown in Fig. 2) is a point absorber wave energy converter [29]. The dimensions of the device are given in Table I [29]. The C4 is selected for this analysis since it is currently one of the state-of-the-art devices, and the closest to achieve commercialisation. Two interesting features of the device are: 1) Wave-spring system [30] which amplifies the motion and power capture of the device by providing a negative spring function, 2) Pre-tensioning system which replaces some of the mass otherwise needed to balance the buoyancy effect and a composite spherical buoy hull structure, that provides high volume with low mass. The device is anchored to the bottom and employs real-time control algorithms to maximize its power output.

The draft of 6 m was assumed by the authors for this study and the natural frequency was calculated based on the aforementioned properties.

#### B. Equation of motion

A frequency domain model was used for estimating the motion of the Corpower C4 device. Only heave



Fig. 2. Corpower C4 wave energy converter device [29]

motion was considered here, with the equation of motion given as follows:

$$[-\omega^2(m_d + m_a) + i\omega(b_a + b_{PTO} + b_v) + c_h]s = f_e \quad (3)$$

where the first 2 terms are the mass of the device  $m_d$  and the added mass heaving hydrodynamic coefficient  $m_a$ . Then,  $b_a$  is the radiation damping heaving hydrodynamic coefficient,  $b_{PTO}$  is the PTO (Power Take Off) coefficient for the device,  $b_v$  is the linearized viscous damping coefficient. Finally,  $c_h$  is the hydrostatic stiffness coefficient in heaving,  $f_e$  is the heave exciting force, and  $s$  is the displacement amplitude of the device also referred to as the body excursion. When the amplitude of the incident wave is 1 m, then  $s$  represents the RAO (Response amplitude Operator) in heave motion for the device.

Within the scope of this formulation, the following interactions have not been considered - (i) the wave spring component of the device which provides a negative spring stiffness and (ii) the pre-tensioning mechanism (iii) the moorings, as the device is anchored to the seabed directly. When considering the control of the device through the PTO system, this is achieved by incorporating two conditions: 1) Cancelling the PTO

TABLE I  
PROPERTIES OF THE CORPOWER C4 DEVICE

Property	Value	Unit
Diameter	9	m
Height	18	m
Installation depth (minimum)	40	m
Weight	70	tonne
Bouy Draft	6	m
Undamped Natural period (heave)	3	s

reactance (also referred to as the stiffness coefficient for the PTO system) which essentially occurs at resonance, and 2) The PTO damping should be equal to the impedance which ensures maximum power absorption. For most practical cases, the PTO reactance is negligible or zero and so considering just the PTO damping condition is sufficient [31]. Therefore, a sub-optimal passive control has been incorporated within the PTO damping coefficient, based on the formulation which takes into account the losses due to viscosity. To determine the viscous losses, a linearized approach has been used.

### C. BEM model

The frequency dependent hydrodynamic coefficients and exciting forces are obtained from the frequency domain Boundary Element Method (BEM) solver HAMS ([32], [33]). Deep water conditions were assumed since the considered depth for comparing the data bases is around 70 m. Convergence studies were conducted during the development of the BEM model to decide on the number of panels.

### D. Sub-optimal PTO control and viscous losses

Sub-optimal passive control including viscous losses was incorporated based on the work of Hals et al. [34]. The optimum PTO damping coefficient for each frequency was derived using (4) without a displacement constraint.

$$b_{PTO}(\omega) = (R_i(\omega)^2 + X_i(\omega)^2)^{1/2} \quad (4)$$

where

$$R_i(\omega) = b_a(\omega) + R_f \quad (5)$$

$$X_i(\omega) = i\omega[m_d + m_a(\omega)] + (c_h/i\omega) \quad (6)$$

$R_i$  and  $X_i$  refer to the real and imaginary part of the intrinsic impedance of the heaving body, with  $R_f$  accounting for the viscous losses. To determine the viscous losses, the methodology from the work of Malta [35] is adopted. The non-linear viscous term based on the Morrison's equation is linearized using a Fourier series expansion.

### E. Power estimation from wave energy converter

The average power produced by the WEC over various sea states is quantified in a power matrix. For its computation, irregular wave sea states based on  $H_s$  and  $T_p$  are considered. For the MREL dataset, the spectra are derived directly from the dataset per sea state, which can then be used to compute the significant heave amplitude ( $\bar{z}_{a_{1/3}}$ ) and average zero-crossing period ( $T_{2z}$ ). Since the spectra was not available to us during the development of this study, for the ERA5 wave data, the JONSWAP spectrum is assumed [36]. It should be noted that the assumption of a parametric spectral shape is typically used in the absence of spectral data (e.g.; [37]).

The significant heave amplitude and average zero-crossing period based on the spectra are obtained as follows:

- Computation of the heave response spectra:

$$S_z(\omega) = |s|^2 * S_\zeta(\omega) \quad (7)$$

where  $s_z(\omega)$  is the heave response spectra,  $s$  is the response amplitude operator and  $S_\zeta(\omega)$  is the input wave spectra (MREL data spectra or JONSWAP).

- Estimation of the zeroth and second moments of the heave response spectra as:

$$m_{nz} = \int_0^\infty S_z(\omega) * \omega^n * d\omega \quad (8)$$

with  $n = 0$  and  $2$ .

- From the moments, the significant heave amplitude and average zero-crossing period can be estimated as:

$$\bar{z}_{a_{1/3}} = 2 * \sqrt{m_{0z}} \quad (9)$$

$$T_{2z} = 2\pi * \sqrt{\frac{m_{0z}}{m_{2z}}} \quad (10)$$

The choice of using the zero-crossing period for the power matrix is based on [37].

The average power based on the heave displacement for a given sea state is obtained using:

$$P = (1/2)\omega_{2z}^2 b_{PTO} \bar{z}_{a_{1/3}}^2 \quad (11)$$

where  $\omega_{2z} = 2\pi/T_{2z}$ .

This power matrix is used together with the scatter diagrams to estimate the yearly power production. Considering the most common  $H_s$  operational ranges, the power matrices used in the in the estimation of power production (in section IV-C), are capped to  $H_s \leq 9$  m.

## IV. RESULTS

### A. Wave heights differences in deep waters

First the wave height fields from ERA5, CFSR and the MREL hindcast with altimeter data are compared. Through the along-track analysis, it is possible to observe within which wave heights' range we can find the most significant differences between these datasets (Fig. 3). The year 2009 was selected since it is the last year available in the CFSR hindcast, which means that a comparison of the 3 databases for more recent years is not possible. In this section, results using only Jason-2 are provided, but the analysis was also done for Jason-1 (with similar results to Jason-2), and Envisat.

Note that in the neighborhood of the most frequent  $H_s$ , around 2 m (Fig. 3.c), the NMB values are similar for all datasets (close to 0%). The CFSR hindcast performs better between wave heights from 4 to 5.5 m, while ERA5 and the MREL hindcast present a slight under estimation (NMB of about -2% ). Most important differences are found for  $H_s > 8$  m, where CFSR and ERA5 present a clear underestimation of the wave heights that tends to increase towards the largest  $H_s$  bins. Note that the NMB of CFSR and ERA5 reaches -19% and -11% respectively at 12.75 m. On the other hand, the MREL hindcast presents a more "controlled" NMB behavior for higher wave heights,

varying between  $-7$  and  $1\%$  (Fig. 3.a). This is mostly due to the wind intensities enhancement applied to the ERA5 wind fields [15].

Since data assimilation is used in the generation of the ERA5 dataset, it is not surprising that the scatter index, along the analyzed  $H_s$  range, is the lowest compared to the other two datasets (Fig. 3.b). Nevertheless, the MREL hindcast presents a SI that is, in average, only  $\sim 3\%$  higher than ERA5 for wave heights between 1.5 to 6 m. Finally, in Fig. 3.c, is possible to observe that the 3 datasets overestimate the occurrences of the most frequent wave heights, between 1.75 and 2.5 m. This effect was partially corrected with adjustments to the swell dissipation parameterization [8] applied in the calibration of the MREL hindcast. In fact, this hindcast presents a smaller over estimation of occurrences in the neighborhood of the peak.

### B. Differences on the offshore wave energy flux

Given the clear differences between the used datasets, it is of interest to verify if these identified characteristics have an impact on the estimation of the wave power density (energy flux). Since the MREL hindcast presents a narrower range of  $H_s$  bias values up to 12.75 m (see Fig. 3.a), this dataset is used as a reference to compare with ERA5 and CFSR. The following expression is used to compute the wave power density:

$$P_{wave} = \frac{\rho_w}{64\pi} (gH_s)^2 T_e \quad (12)$$

where  $\rho_w$  is the water density, here taken as  $1.026 \text{ kg/m}^3$ ,  $g$  is the acceleration of gravity ( $9.81 \text{ m/s}^2$ ), and  $T_e$  the energy period. Although  $T_e$  here is estimated as  $0.9T_p$ , with  $T_p$  obtained from the used datasets, its value normally varies depending on local sea states characteristics (e.g.; [3], [38]).

In Fig. 4, it is possible to observe clear discrepancies on the offshore energy flux. Note that all these comparisons are done with respect to the N\_ATL-15M grid (see Fig. 1). Starting from deep waters, between longitudes  $-12^\circ$  and  $-20^\circ$ , the ERA5 product already shows differences that can be  $\geq -5\%$  compared to the MREL hindcast (Fig. 4.b). On the other hand, when comparing with CFSR in this area, NMD are typically  $< 5\%$  and actually closer to  $0\%$  (Fig. 4.c). Larger differences are normally found within the coastal shelf, where NMD values can be  $> -20\%$  (for example at Portugal and the Bay of Biscay). This is mainly attributed to the coarser spatial resolution from ERA5 and CFSR. Given the higher resolution of the the MREL model, it is expected that some bathymetric features are better resolved for depths  $< 500 \text{ m}$  (e.g.; [26]).

Particularly interesting are the differences within the North Sea. Probably because the MREL hindcast is forced by ERA5 winds, NMD are smaller than those obtained with CFSR, which are in average  $> 10\%$  and can be  $> 20\%$  in shallower areas.

### C. Estimation of the mean absorbed power

In section IV-B it was verified how estimations of the offshore energy flux may vary depending on the

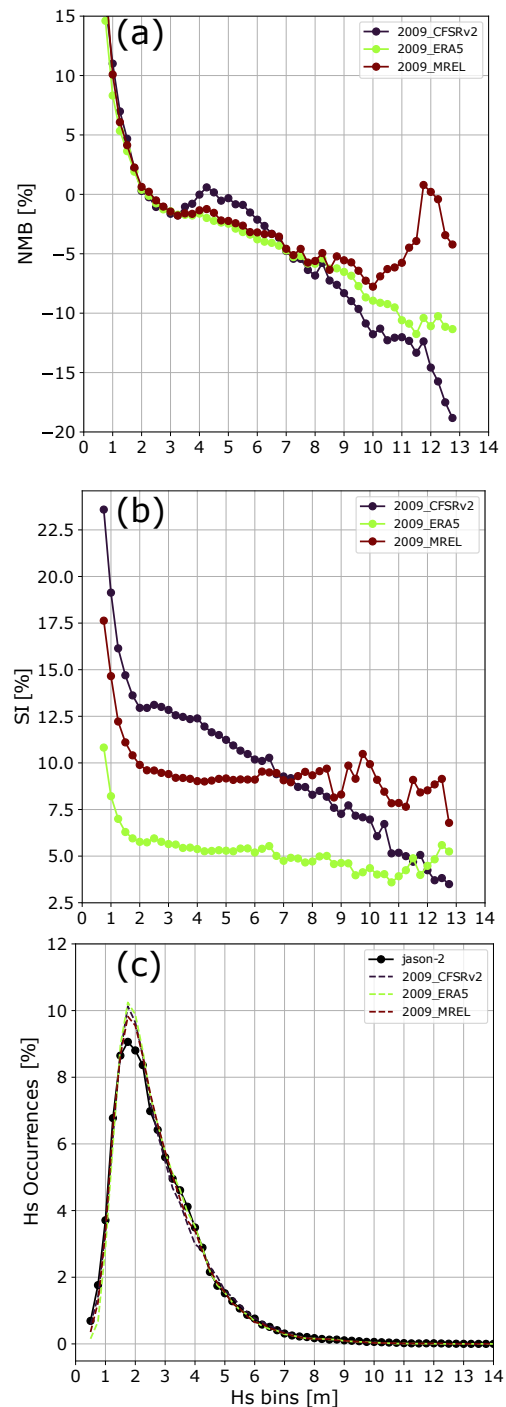


Fig. 3. (a) Normalized mean bias (NMB), (b) Scatter index (SI) and (c)  $H_s$  distribution computed for year 2009 using Jason-2 altimeter. Results in (a) and (b) are model-altimeter. Bin size is 0.25 m.

used wave dataset. These differences, mainly caused by the combination of forcing fields, physical parameterizations and numerical choices will indeed have an effect on the power production estimations. Regardless of their suitability, the typically available  $H_s$  and  $T_p$  information from “global” datasets is commonly used for a first estimation of the power production for a specific location. It is thus of interest to quantify the changes in the estimated power production using wave datasets with different characteristics.

In the present section, the power production for

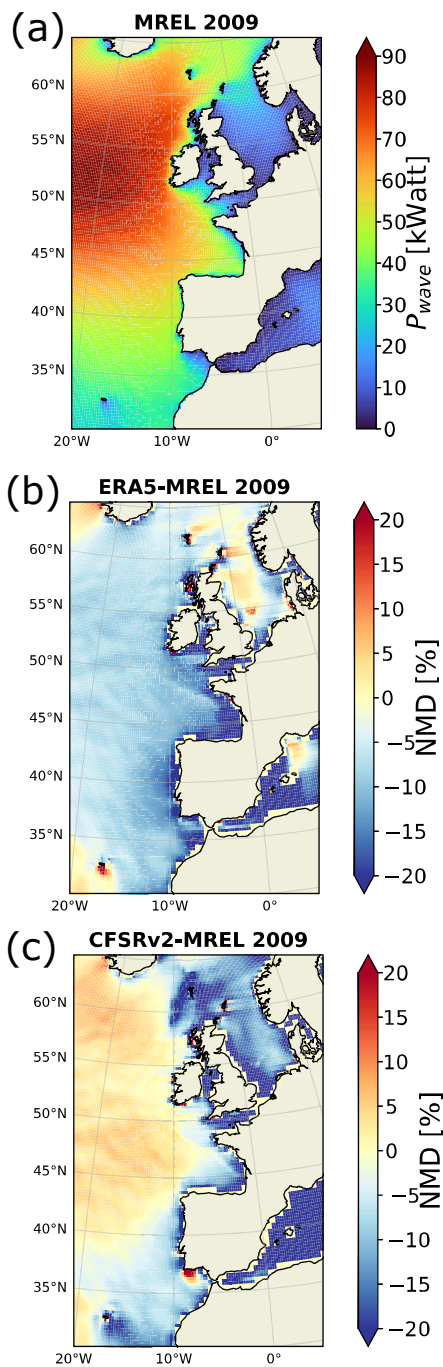


Fig. 4. Mean  $P_{wave}$  in kWatt obtained with MREL hindcast (N\_ATL-15M grid) for 2009 in (a), and Normalized Mean Differences (NMD) compared with ERA5 in (b) and CFSR hindcast in (c).

year 2009 is computed using the ERA5 wave product and the MREL hindcast. The analysis is performed for a location identified as MREL-AGU, off the coast of Aguçadoura in Portugal at 70.4 m depth (longitude:  $-8.95^\circ$ , latitude:  $41.47^\circ$ ; see Fig. 5.a). To compare, the ERA5  $H_s$  and  $T_p$  fields are interpolated into the MREL-AGU location to create the ERA5-AGU time series. Note that the closest ERA5 grid point is about 7.5 km away from MREL-AGU, at a similar depth ( $\sim 80$  m).

First, using the times series from the analyzed location, the  $H_s$ - $T_p$  distributions are computed (Fig. 5.b,c). For both datasets the overall  $T_p$  occurrences' peak is located between 12 and 12.5 s but with clear different occurrences (19% for ERA5 and 11.5% for MREL

respectively). Additionally, MREL-AGU presents particularly large occurrences (4.56%) at ( $H_s=1.5$ ,  $T_p=8.5$ ) which could be partially attributed to a higher overall dissipation in the parameterization for atmospheric-sea surface interactions [8]. We also note a comparatively larger amount of occurrences of  $H_s$  between 6 and 8 m at MREL-AGU (Fig. 5.b).

As explained in section III, to estimate the power absorbed, the power matrix of the PA-WEC was computed for the specific depth of the analyzed location. The power matrix for MREL-AGU was derived using the average of the corresponding spectra from each  $H_s$ - $T_p$  combination assigned at a given bin range. With this approach it is expected to better represent the mean sea state conditions related to every  $H_s$ - $T_p$  bin (e.g. see Fig. 6). For ERA5-AGU, the spectral shape at each bin is obtained applying the  $H_s$  and  $T_p$  bin marks to the JONSWAP spectrum formulation assuming a  $\gamma$  shape factor of 3.3.

With these considerations, a mean absorbed power of 12.86 kW is estimated when using the MREL hindcast at the analyzed location (MREL-AGU) for 2009. With the generated time series at the same location, from the ERA5  $H_s$  and  $T_p$  fields, the estimated mean absorbed power is 10.53 kW.

## V. CONCLUSION

In the preset study we first analyzed the differences between 3 wave datasets (ERA5, CFSR and MREL) and how their particular characteristics affect the estimation of the offshore energy flux. Then, a preliminary analysis to verify how the sea states' characteristics in deep waters affect the estimations of the absorbed power from a PA-WEC in intermediate water depths is included.

The 3 databases compared present similar bias levels in the neighborhood of 2 m  $H_s$ . Nevertheless, the MREL hindcast shows an overall narrower range of NMB changes compared to altimeter data from the CCI Sea State V3 product. Particularly for  $H_s > 8$  m, the MREL dataset performs better than the ERA5 reanalysis and the CFSR hindcast as the underestimation of wave heights has been reduced. This is due to the specific adjustments to the wind-wave growth term in the ocean-atmosphere parameterization and corrections to the low intensity bias in the ERA5 wind product. Additionally, adjustments in the swell dissipation parameterization helped to improve the wave heights distribution in the North-East Atlantic. With these changes, a slight reduction of the occurrences' overestimation of  $H_s$  between 1.75 and 2 m is obtained (which is still better than ERA5 and CFSR).

Taking the MREL hindcast as reference, differences of the offshore energy flux in deep waters can be  $> -5\%$  between ERA5 and MREL and  $< 5\%$  when comparing with CFSR. Larger differences are found within the European coastal shelf where, in general, differences can be  $> -20\%$  comparing with ERA5 or CFSR. In this case, the higher resolution of the N\_ATL-15M grid, and the feedback from the high resolution grids in the multi-grid MREL model setup, help to better represent the wave field evolution in this area.

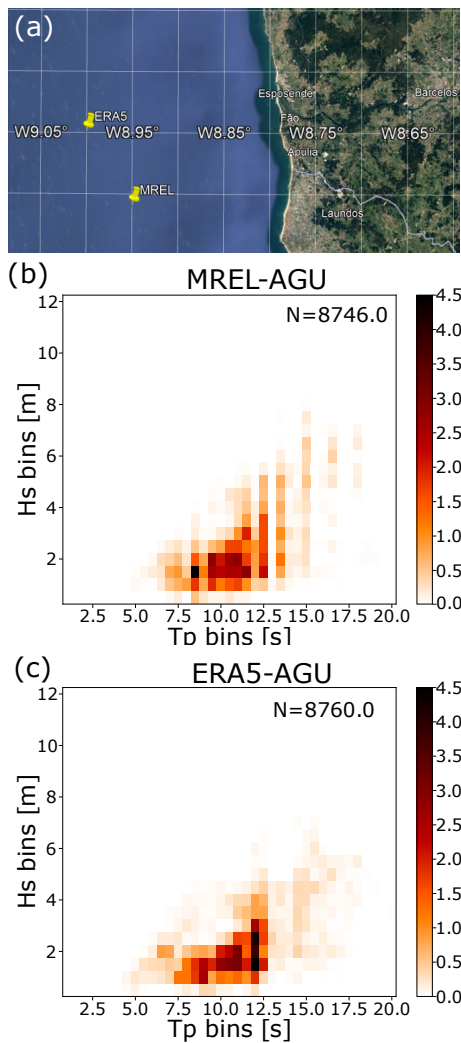


Fig. 5. In (a) Output location of MREL-AGU spectra time series and closest ERA5 node for 2009.  $H_s$ - $T_p$  bi-variate distributions for MREL-AGU output time series in (b), and for ERA5 data interpolated into MREL-AGU coordinates in (c).  $H_s$  bin size is 0.5 m and  $T_p$  bin size is 0.5 s.  $N$  is the total amount of analyzed data. The analyzed  $H_s$  range is from 0.5 to 14 m, while the analyzed  $T_p$  range covers from 1 to 20 s. Map data in (a) taken from ©Google Landast / Copernicus. Colorbars in (b) and (c) show occurrences in %.

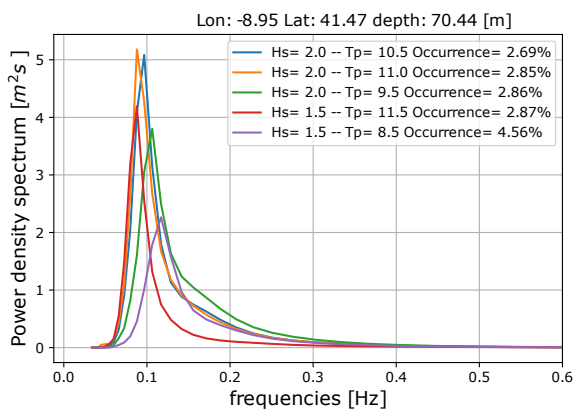


Fig. 6. Mean spectrum of the 5 most frequent  $H_s$ - $T_p$  combinations from MREL-AGU for 2009.

It should be mentioned that the hindcast developed by the authors has already undergone 2 phases of validation. First with altimeter data (e.g.; Fig. 3) and then

with buoy data in deep waters (not shown here) from CMEMS in Situ TAC (Thematic Assembly Center). Validation with buoys (e.g.; 6200084, 6200029, 6200095, 6200105, to name a few) showed  $H_s$  correlations  $\geq 0.96$ , with bias ranging from -2 to 2%. For  $T_p$  correlations are typically  $\geq 0.78$  with bias ranging from 0.14 to  $\sim 5\%$  depending on the location (and probably the instrument recording characteristics). Based on these results, it is thought that the use of the MREL hindcast as reference to compare with the other datasets is adequate given its proven accuracy level.

Finally, using a PA-WEC power matrix specially computed for the analyzed location, it was verified that the difference of the mean absorbed power for 1 year (2009) can be of about 20%. In this case, between wave data from the MREL hindcast compared to ERA5. Since the MREL hindcast multi-grid setup has higher spatial resolution in the coastal shelf (N\_ATL-8M and EU-2M grids), and considers tidal forcing, the sea states evolution is better represented. Thus, it is expected that the obtained joint  $H_s$ - $T_p$  distributions are more accurate than the ones obtained from ERA5 at intermediate waters. Hence, the power estimates are also considered to be more realistic at MREL-AGU, specially when the corresponding spectra related to each ( $H_s$ ,  $T_p$ ) bin range is used.

It should be again highlighted that only the heave motion of the PA-WEC has been considered in the generation of the power matrices. Adding the surge changes the response of the device, and the estimated power captured might increase depending on the local wave field characteristics. Although, in intermediate to deep water conditions, the contribution of the heave is expected to be dominant.

The generation of a 30 years high resolution hindcast for European waters (including the Mediterranean and Baltic seas) is an ongoing work, as well as its validation in shallower depths.

#### ACKNOWLEDGEMENT

This study has been conducted using E.U. Copernicus Marine Service Information (<https://doi.org/10.48670/moi-00050>, <https://doi.org/10.48670/moi-00059>). The work has been a part of the EU-SCORES project that has received funding from the European Union's Horizon 2020 research and innovation programme under grant agreement No 101036457.

#### REFERENCES

- [1] F. Lucero, P. A. Catalán, Á. Ossandón, J. Beyá, A. Puelma, and L. Zamorano, "Wave energy assessment in the central-south coast of Chile," *Renewable Energy*, vol. 114, pp. 120–131, 2017.
- [2] G. Lavidas and V. Venugopal, "Application of numerical wave models at European coastlines: A review," *Renewable and Sustainable Energy Reviews*, vol. 92, pp. 489–500, 2018. [Online]. Available: <https://doi.org/10.1016/j.rser.2018.04.112>
- [3] N. Guillou, G. Lavidas, and G. Chapalain, "Wave energy resource assessment for exploitation—a review," *Journal of Marine Science and Engineering*, vol. 8, no. 9, p. 705, 2020.
- [4] R. P. Patel, G. Nagababu, S. V. A. Kumar, M. Seemanth, and S. S. Kachhwaha, "Wave resource assessment and wave energy exploitation along the Indian coast," *Ocean Engineering*, vol. 217, p. 107834, 2020.

- [5] N. Li, G. García-Medina, K. F. Cheung, and Z. Yang, "Wave energy resources assessment for the multi-modal sea state of hawaii," *Renewable Energy*, vol. 174, pp. 1036–1055, 2021.
- [6] J. Morim *et al.*, "A global ensemble of ocean wave climate statistics from contemporary wave reanalysis and hindcasts," *Scientific data*, vol. 9, no. 1, p. 358, 2022.
- [7] L. Cavaleri and L. Bertotti, "In search of the correct wind and wave fields in a minor basin," *Monthly Weather Review*, vol. 125, no. 8, pp. 1964–1975, 1997. [Online]. Available: <http://ams.allenpress.com/archive/1520-0493/125/11/pdf/i1520-0493-125-8-1964.pdf>
- [8] F. Ardhuin *et al.*, "Semi-empirical dissipation source functions for wind-wave models: part I, definition, calibration and validation," *Journal of Physical Oceanography*, vol. 40, no. 9, pp. 1917–1941, 2010.
- [9] H. L. Tolman, "On the selection of propagation schemes for a spectral wind wave model," NWS/NCEP, Office Note 411, 1995, 30 pp + figures.
- [10] A. Roland and F. Ardhuin, "On the developments of spectral wave models: numerics and parameterizations for the coastal ocean," *Ocean Dynamics*, vol. 64, no. 6, pp. 833–846, 2014.
- [11] H. Hersbach *et al.*, "The ERA5 global reanalysis," *Quart. Journ. Roy. Meteorol. Soc.*, vol. 146, pp. 1999–2049, 2020.
- [12] A. Chawla, D. Spindler, and H. L. Tolman, "A thirty year wave hindcast using the latest ncep climate forecast system reanalysis winds," in *Proc. 12th Int. Workshop on Wave Hindcasting and Forecasting*, vol. 310, 2011.
- [13] A. Chawla, D. M. Spindler, and H. L. Tolman, "Validation of a thirty year wave hindcast using the climate forecast system reanalysis winds," *Ocean Modelling*, vol. 70, pp. 189–206, 2013.
- [14] The WAVEWATCH III<sup>®</sup> Development Group, "User manual and system documentation of WAVEWATCH III<sup>®</sup> version 6.07 [Software]," NOAA/NWS/NCEP/MMAB, College Park, MD, USA, Tech. Note 333, 2019, 465 pp. + Appendices.
- [15] M. Alday, M. Accensi, F. Ardhuin, and G. Dodet, "A global wave parameter database for geophysical applications. part 3: Improved forcing and spectral resolution," *Ocean Modelling*, vol. 166, p. 101848, 2021.
- [16] J.-F. Piollé, G. Dodet, Y. Quilfen, M. Schwatke, C. and Passaro, G. Quartly, and P. Thibaut, "Esa sea state climate change initiative (sea\_state\_cci): Global remote sensing multi-mission along-track significant wave height from altimetry, l2p product, version 3," *NERC EDS Centre for Environmental Data Analysis*, 2022.
- [17] H. L. Tolman, "A mosaic approach to wind wave modeling," *Ocean Modelling*, vol. 25, pp. 35–47, 2008.
- [18] A. Chawla, H. L. Tolman, V. Gerald, D. Spindler, T. Spindler, J.-H. G. M. Alves, D. Cao, J. L. Hanson, and E.-M. Devalliere, "A multigrid wave forecasting model: A new paradigm in operational wave forecasting," *Weather and Forecasting*, vol. 28, pp. 1057–1078, 2013.
- [19] F. Girard-Ardhuin and R. Ezraty, "Enhanced arctic sea ice drift estimation merging radiometer and scatterometer data," *IEEE Transactions on Geoscience and Remote Sensing*, vol. 50, pp. 2639–2648, 2012.
- [20] L. Pineau-Guillou, F. Ardhuin, M.-N. Bouin, J.-L. Redelsperger, B. Chapron, J. Bidlot, and Y. Quilfen, "Strong winds in a coupled wave-atmosphere model during a north Atlantic storm event: evaluation against observations," *Quart. Journ. Roy. Meteorol. Soc.*, vol. 144, pp. 317–332, 2018.
- [21] S. Hasselmann and K. Hasselmann, "Computation and parameterizations of the nonlinear energy transfer in a gravity-wave spectrum. part I: a new method for efficient computations of the exact nonlinear transfer," *Journal of Physical Oceanography*, vol. 15, pp. 1369–1377, 1985.
- [22] WAMDI Group, "The WAM model - a third generation ocean wave prediction model," *Journal of Physical Oceanography*, vol. 18, pp. 1775–1810, 1988. [Online]. Available: <http://journals.ametsoc.org/doi/pdf/10.1175/1520-0485%281988%29018%3C1775%3ATWMTGO%3E2.0.CO%3B2>
- [23] D. M. Spindler, A. Chawla, and H. L. Tolman, "An initial look at the cfsr reanalysis winds for wave modeling," *Technical note, mmab contribution*, no. 290, 2011.
- [24] F. Schlembach *et al.*, "Round robin assessment of radar altimeter low resolution mode and delay-doppler retracking algorithms for significant wave height," *Remote Sensing*, vol. 12, no. 8, 2020. [Online]. Available: <https://www.mdpi.com/2072-4292/12/8/1254>
- [25] M. Passaro, M. A. Hemer, G. D. Quartly, C. Schwatke, D. Dettmerring, and F. Seitz, "Global coastal attenuation of wind-waves observed with radar altimetry," *Nature Communications*, vol. 12, no. 1, pp. 1–13, 2021.
- [26] M. Alday, F. Ardhuin, G. Dodet, and M. Accensi, "Accuracy of numerical wave model results: Application to the atlantic coasts of europe," *Ocean Science*, vol. 18, no. 6, pp. 1665–1689, 2022.
- [27] W. H. F. Smith and R. Scharroo, "Waveform aliasing in satellite radar altimetry," *IEEE Transactions on Geoscience and Remote Sensing*, vol. 53, pp. 1671–1682, 2015.
- [28] F. Ardhuin *et al.*, "Observing sea states," *Frontiers in Marine Science*, vol. 6, p. 124, 2019.
- [29] (2023) Corpover. [Online]. Available: <https://corpoverocean.com/wave-energy-technology/>
- [30] J. Hals, G. S. Ásgeirsson, E. Hjalmarsson, J. Maillet, P. Möller, M. Guérinel, and M. Lopes, "Tank testing of an inherently phase-controlled wave energy converter," *International Journal of Marine Energy*, vol. 15, pp. 68–84, 2016, selected Papers from the European Wave and Tidal Energy Conference 2015, Nantes, France. [Online]. Available: <https://www.sciencedirect.com/science/article/pii/S2214166916300182>
- [31] M. Alves, "Chapter 2 - frequency-domain models," in *Numerical Modelling of Wave Energy Converters*, M. Folley, Ed. Academic Press, 2016, pp. 11–30. [Online]. Available: <https://www.sciencedirect.com/science/article/pii/B9780128032107000025>
- [32] Y. Liu, "HAMS: A frequency-domain preprocessor for wave-structure interactions—theory, development, and application," *Journal of Marine Science and Engineering*, vol. 7, no. 3, 2019. [Online]. Available: <https://www.mdpi.com/2077-1312/7/3/81>
- [33] V. Raghavan, G. Lavidas, A. Metrikine, N. Mantadakis, and E. Loukogeorgaki, "A comparative study on BEM solvers for wave energy converters." CRC Press, 10 2022, pp. 441–447. [Online]. Available: <https://www.taylorfrancis.com/books/9781003360773/chapters/10.1201/9781003360773-50>
- [34] J. Hals, T. Bjarte-Larsson, and J. Falnes, "Optimum Reactive Control and Control by Latching of a Wave-Absorbing Semisubmerged Heaving Sphere," vol. 21st International Conference on Offshore Mechanics and Arctic Engineering, Volume 4, pp. 415–423, 06 2002. [Online]. Available: <https://doi.org/10.1115/OMAE2002-28172>
- [35] E. B. Malta, R. T. Goncalves, F. T. Matsumoto, F. R. Pereira, A. L. C. Fajarra, and K. Nishimoto, "Damping Coefficient Analyses for Floating Offshore Structures," vol. 29th International Conference on Ocean, Offshore and Arctic Engineering: Volume 1, pp. 83–89, 06 2010. [Online]. Available: <https://doi.org/10.1115/OMAE2010-20093>
- [36] O. M. Mazzaretto, M. Menéndez, and H. Lobeto, "A global evaluation of the jonswap spectra suitability on coastal areas," *Ocean Engineering*, vol. 266, p. 112756, 2022. [Online]. Available: <https://www.sciencedirect.com/science/article/pii/S002980182202039X>
- [37] M. Penalba, A. Ulazia, G. Ibarra-Berastegui, J. Ringwood, and J. Sáenz, "Wave energy resource variation off the west coast of ireland and its impact on realistic wave energy converters' power absorption," *Applied Energy*, vol. 224, pp. 205–219, 2018. [Online]. Available: <https://www.sciencedirect.com/science/article/pii/S0306261918306895>
- [38] N. Guillou, "Estimating wave energy flux from significant wave height and peak period," *Renewable Energy*, vol. 155, pp. 1383–1393, 8 2020.